PNAS RESEARCH ARTICLE | EVOLUTION

Parallel sensory compensation following independent subterranean colonization by groundwater salamanders (*Eurycea*)

Ruben U. Tovar[a], Brittany A. Dobbins[a,b], Nicholas R. Hartman[a], Sheena Leelani[a], Thomas J. Devitt[a], Dana M. García[b], Paul M. Gignac[c], David C. Cannatella[a], and David M. Hillis[a,1]

Affiliations are included on p. 9.

Contributed by David M. Hillis; received March 6, 2025; accepted April 23, 2025; reviewed by James Hanken and William R. Jeffery

Lineages that have invaded subterranean environments have repeatedly evolved remarkable adaptations to life in darkness. However, observational and experimental studies in additional natural systems are needed to further our understanding of repeated evolution and convergence. In Texas, a radiation of groundwater salamanders (genus *Eurycea*), with independent invasions of subterranean karstic environments, offers an opportunity to investigate phenotypic convergence, parallel evolution, and the enhancement and regression of sensory systems. Adaptations to a troglobitic life in this clade include morphological, behavioral, and physiological changes within and among species. Intraspecific and interspecific variation in morphology in response to the selective pressures of life underground allows for detailed examination of physical, behavioral, and physiological changes associated with subterranean adaptation within a comparative phylogenetic framework. We find a correlated change between two sensory systems repeated across multiple subterranean *Eurycea* lineages: the degeneration of the eye and the expansion of the mechanosensory lateral line. The increase in anterior neuromast organs in subterranean lineages was positively correlated with the expression of *pax6* (Paired-box 6), a conserved transcription factor important for vertebrate neurogenesis. Our results show a decreasing trend of PAX6 labeling in the neuromasts of adult surface salamanders (*Eurycea nana*) relative to the maintained labeling in subterranean species (*Eurycea rathbuni*). These lateral line enhancements are correlated with reductions in the development of optic systems in subterranean salamander lineages. Altogether, our findings provide a starting point for future evolutionary developmental investigations examining the genetic underpinnings of adaptive, repeated evolution in a novel system.

adaptive evolution | convergence | development | parallel evolution | sensory systems

Significance

Underexplored subterranean environments in Central Texas harbor a phenotypically and taxonomically diverse radiation of groundwater salamanders, which we used to test the molecular and developmental bases for adaptive evolution in extreme environments. Using an integrative approach, we quantify the divergence and convergence of two sensory modalities: vision loss and mechanoreception. The divergent developmental and phenotypic changes have evolved several times in parallel among populations and species in this group. Understanding the evolutionary developmental processes responsible for these shifts will further our understanding of adaptive, repeated evolution in a natural system.

Colonization of new environments can exert strong selective pressures on organisms, leading to new adaptive behaviors or traits (1). Subterranean habitats are considered extreme because they have little to no light and often limited food resources due to the lack of primary productivity (2). Organisms inhabiting these environments—termed stygofauna—are under common selective pressures that result in phenotypic convergence upon a suite of features characteristic of subterranean organisms, including reduced or absent eyes, reduced number of melanophores, elongation of appendages, and craniofacial modifications (3–6). In closely related lineages, shared phenotypes may result from parallel evolution in response to these common environmental pressures (7–10). Globally, stygofauna are represented by diverse metazoan taxa; among vertebrates, only teleost fishes (11–14) and salamanders (4) have evolved stygobitic forms.

The karstic Edwards–Trinity aquifer system of west-central Texas, USA, is a vast network of subterranean aquifers comprised mainly of sandstone in the lower portions and porous limestone in the upper portions (15) with abundant surface springs. Weakly acidic precipitation facilitated the dissolution of Cretaceous limestone across the Balcones Fault Zone along the southern Edwards Plateau region. Since the Miocene, subterranean habitats have gradually formed from both geologic and hydrologic events. Climatic oscillations of alternating increased precipitation and drought (16) are associated with the evolution of an exceptionally diverse regional stygofauna.

The Edwards–Trinity groundwater ecosystem is home to 15 species of paedomorphic salamanders in the genus *Eurycea* (clade *Paedomolge*; 17). These salamanders are permanently aquatic and neotenic, retaining juvenile features into adulthood, including external gills and a broad tail fin. Some species are found in surface springs (e.g., *Eurycea sosorum* and *Eurycea nana*). One clade (the subgenus *Typhlomolge*) contains obligately subterranean species (*Eurycea rathbuni*, *Eurycea robusta*, *Eurycea waterlooensis,* and an undescribed

Reviewers: J.H., Harvard University; and W.R.J., University of Maryland.

Competing interest statement: James Hanken (Reviewer 1), David Hillis (corresponding author of this paper), and David Cannatella (a contributing author of this paper) were 3 of 120 co-authors of a formal statement titled "Specimen collection is essential for modern science", published in *PLoS Biol.* **21**(11): e3002318. https://doi.org/10.1371/journal.pbio.3002318. This statement was not a research paper, and none of these authors have had any research or other collaborations in the past decade. The formal statement was a note on the importance of museum specimens, and each of us signed onto the statement independently. The statement included many of the museum-associated researchers in North America.

[1]To whom correspondence may be addressed. Email: dhillis@austin.utexas.edu.

This article contains supporting information online at https://www.pnas.org/lookup/suppl/doi:10.1073/pnas.2504850122/-/DCSupplemental.

Published June 3, 2025.

species). Other species, including *Eurycea latitans*, *Eurycea pterophila*, and *Eurycea troglodytes*, inhabit both subterranean and surface spring habitats. Surface populations and species have fully pigmented skin and well-developed eyes. In contrast, obligately subterranean species exhibit features widely considered to be cave adaptations, such as a broad, flattened head, wide mouth, elongated limbs, greatly reduced numbers of melanophores, and vestigial eyes (6, 17–20). Species that have both surface and subterranean populations are highly variable in their subterranean-adapted traits (21); some populations lack melanophores and contain eyeless individuals but do not exhibit the extreme troglomorphism that characterizes *Typhlomolge* species, including dorsoventrally compressed head. These polymorphic populations offer exceptional potential for identifying whether cave colonization is facilitated by genetic background, phenotypic plasticity, or both (22). Importantly, phylogenetic analyses support a history of repeated, independent colonization of subterranean habitats in *Paedomolge* (23–26 and Fig. 1), which offers a compelling system for investigating the evolutionary developmental basis of adaptive evolution by quantifying the phenotypic changes that occur following colonization of an environment devoid of light.

The degeneration or loss of eyes is one of the most salient features of cave-adapted organisms. Descriptions of subterranean salamander species have broadly categorized reduced eyes and pigmentation as convergent phenotypes (4). However, ocular and lateral line development show similarities across most vertebrates (27). Even eye formation in the Mexican blind tetra (*Astyanax mexicanus*) is developmentally conserved (5, 7), although it resides

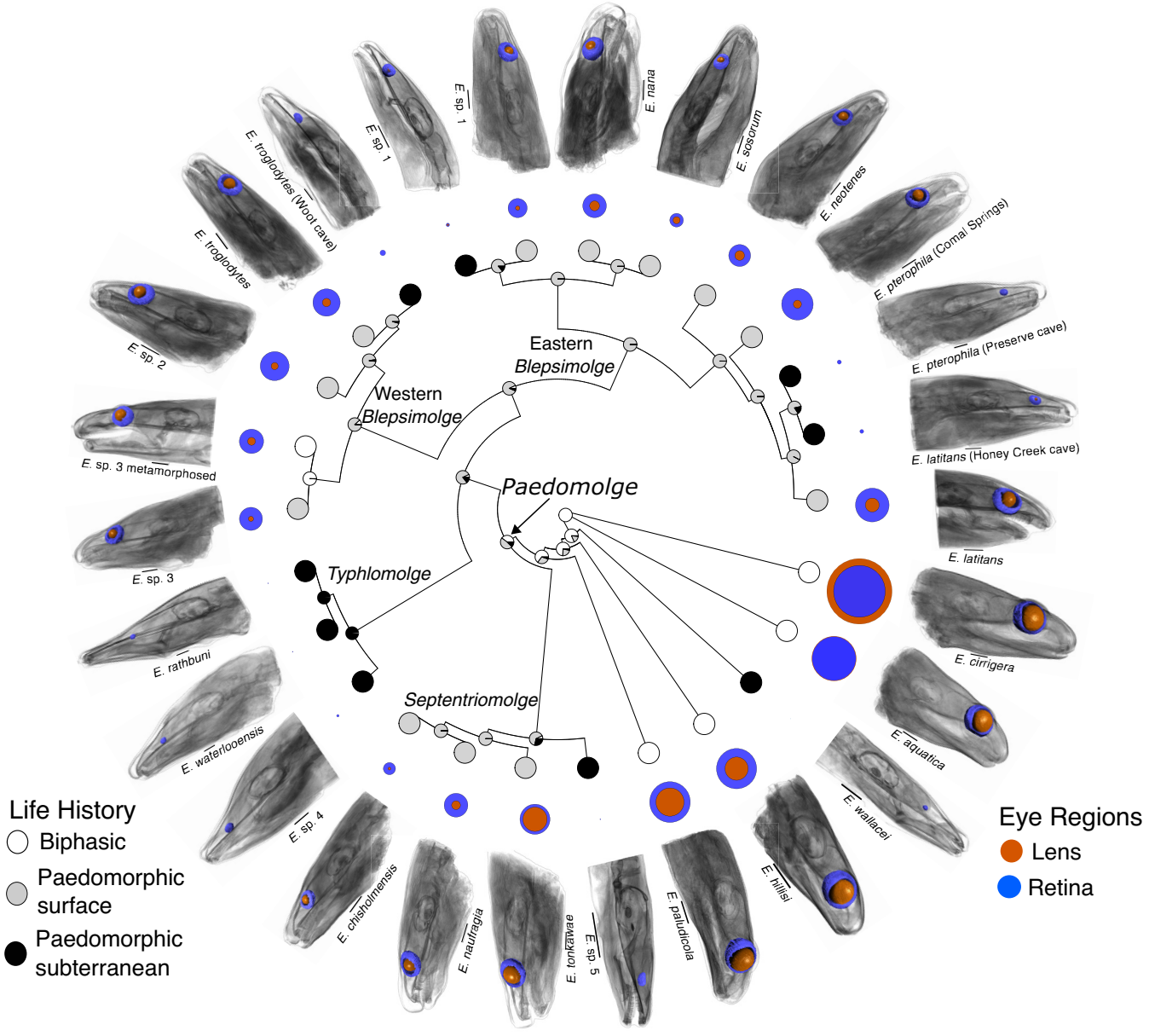

Fig. 1. A phylogeny based on *cytochrome b* and *RAG 1* gene sequences. The reconstructed ancestral states were inferred from a one-rate model. Three life history states—biphasic (white circles), paedomorphic surface (gray circles), and paedomorphic subterranean (black circles)—were estimated and mapped onto each node. Six subterranean invasions are inferred within *Paedomolge*, at least one within each subclade (*Septentriomolge*, *Typhlomolge*, and the Eastern and Western *Blepsimolge*), and one outside this group (*E. wallacei*). The diameters of the lens and retina of each species are shown on the respective salamander heads; the diameter of the retina is always larger than diameter of the lens. The relative volumes of each eye region are plotted in nested circles around the perimeter of the phylogeny. The retinal volume (blue) is typically larger than the lens volume (orange) with the exception of *E. aquatica* and *E. cirrigera*, where the inverse is true (in *E. aquatica* the lens is only marginally larger in volume). Most subterranean species lack a lens. DiceCT scans of exemplar heads follow the eye volume measurements and show the relative position and size in situ. (Scale bars indicate 1 mm.)

in complete darkness. Similar developmental conservation between the subterranean and surface *A. mexicanus* is also observed. However, eye developmental patterns diverge when cessation of growth and eventual apoptosis is initiated by the early-differential expression of Sonic Hedgehog (*shh*) compared to Paired box protein 6 (*pax6*) (7) in subterranean populations of *A. mexicanus*.

In salamanders, differing degrees of ocular regression are especially obvious in cave-adapted species of *Eurycea*, *Typhlotriton*, and *Proteus* (28–31). Although early developmental canalization of the vertebrate eye has been observed in several subterranean and fossorial species (7, 31, 32), the complex pathways by which functional eyes form include numerous opportunities for disruption. Thus, eye degeneration and loss may occur by different mechanisms among lineages (7, 32, 33). These mechanisms may leave the underdeveloped eyes in different stages of regression, but such a phenomenon has not been explored in a comparative framework in salamanders.

Without functional eyes, selection may enhance other sensory systems important in navigation, predator–prey interactions, and mate recognition as a compensatory mechanism (1, 34–36). The lateral line, a mechanosensory system present in fish and most larval amphibians, is likely to undergo compensatory evolution (37, 38). The lateral line system contains a series of epithelial mechanoreceptor organs (neuromasts; 39) found superficially (skin surface) in larval amphibians, or both superficially and in modified canals in fishes. Neuromasts respond to water pressure and movement (38). Inside each neuromast is a cluster of hair cells (*SI Appendix*, Fig. S1). From the apical portion of each hair cell projects tiered rows of stereocilia and a single kinocilium (*SI Appendix*, Fig. S2), extending into a jelly-like dome known as the cupula (40). Disturbances in the water create pressure waves that displace the cupula and bend the embedded cilia. The movement of the cilia results in changes in the membrane potential of the hair cell, which is communicated to attendant neurons and then to the brain. The lateral line system includes the anterior lateral line (ALL), which contains neuromasts of the head, and the posterior lateral line (PLL), comprising trunk and tail neuromasts. In the Mexican blind tetra (*A. mexicanus*), there is variation in neuromast counts among populations; some subterranean populations have more ALL neuromasts than others, which in turn have more than their sighted, surface-dwelling ancestors (5, 7, 12, 36–38).

Aquatic salamanders have hundreds of neuromasts, making the lateral line system an important, nonvisual sensory system (40, 41). Whether subterranean-adapted salamanders have expanded their lateral line in a similar fashion to cavefish has not been previously explored. To investigate whether eye degeneration and loss in *Eurycea* is correlated with expansion of the lateral line system, we quantified eye volume and the number and location of superficial neuromasts in developmental series of multiple surface and subterranean populations and species. We predicted that subterranean salamanders would show parallel trends in both eye reduction and exhibit more neuromasts than surface species, with obligately subterranean species (*Typhlomolge*) showing the greatest degree of expansion.

Results

Phylogeny Estimation. Our phylogeny estimate is consistent with others (42); a clade of paedomorphic species (*Paedomolge*) includes both surface and subterranean species, and some currently recognized species have populations with surface and subterranean ecotypes. Although we constructed an ultrametric tree, we did not time-calibrate it. However, a comparison to Stewart et al. (42) suggests that *Paedomolge* diverged from other *Eurycea* about 23 Mya and subsequently diversified 19 Mya.

Evolutionary Patterns in Life History Traits (Ecotypes). To quantify the rate of evolutionary shifts among the three ecotypes and to estimate ancestral conditions on the phylogeny, we reconstructed ancestral states using four Mk models (43): one rate, six rate, ordered, and irreversible. We repeated these four analyses, adding a rate-heterogeneity (gamma) parameter to the models (see *SI Appendix*, Table S1 and Methods for details and comparison of the models). Based on the weighted Akaike Information Criterion (44), the one-rate model with rate heterogeneity was selected because it showed the best fit to the data (*SI Appendix*, Table S1), although the other models gave qualitatively similar results (*SI Appendix*, Table S2).

The transition from biphasic life history to paedomorphy occurred early during the divergence of *Paedomolge* (Fig. 1). At least six subterranean invasions occurred within the clade, probably in the last 3 My, and at least one subterranean lineage is represented within each named subclade (Fig. 1). We infer this by adding stochastic character mapping (45, *SI Appendix*, Table S2) for the range of estimates of life history state transitions from the models we examined.

Shape Differences and Homoplasy among Ecotypes. Our analyses of continuous variation in shape variables included exploratory plots (*SI Appendix*, Figs. S3–S5), assessment of phylogenetic signal, principal components (standard and phylogenetic) to explore overall shape differences among ecotypes, ANOVA and ANCOVA (standard and phylogenetic) tests of differences among ecotypes, and ancestral state reconstruction.

Phylogenetic signal in a trait is the tendency for related species to resemble each other more than they would if the trait were evolving at random. If the trait is evolving under Brownian motion, where phylogenetic signal should be high, then lambda equals 1. We assessed phylogenetic signal of raw morphometric variables and principal component scores using Pagel's lambda (46) where 0 indicates no signal and 1 indicates strong signal; that is, the trait evolution tracks the phylogeny. Using likelihood-ratio tests, we tested the hypothesis that lambda = 1.0 and rejected it ($P < 0.05$) for the three eye variables, all three standard principal components, and two of the three phylogenetic principal components (*SI Appendix*, Table S3). We conclude that the size and shape of the retina and lens are not reliable indicators of phylogenetic relationships.

We performed both standard (nonphylogenetic) principal component analysis (PCA) and a phylogenetic PCA (47) of the species means for Retina Total Volume, Lens Total Volume, and Snout–Gular length (a proxy for body size). The PCA shows that the first two axes explain 95% of the variance (*SI Appendix*, Fig. S6*A*). For all components of the phylogenetic principal component analyses (PPCA), the interpretation of loadings and eigenvectors is almost identical to that of the PCA, so we discuss only the PCA (*SI Appendix*, Table S4). PC 1 of the PCA is interpreted as a size factor because all loadings are positive (*SI Appendix*, Table S4). The ecotypes are easily separated along this axis (*SI Appendix*, Fig. S6*A*). PC 2 is a contrast between head size (SGL) and overall eye size (Lens Total Volume plus Retina Total Volume); species such as *E. waterlooensis* have large heads compared to their eye size (high score on PC 2). The subterranean species have low scores on PC 1 (overall small eyes) but span the entire range of PC 2 scores. PC 3, which explains only 4% of the variance, nonetheless separates the surface and subterranean species (*SI Appendix*, Fig. S6 *B* and *C*); it is a contrast between Retina Total Volume and Lens Total Volume. Positive scores indicate a retina that is large relative to the lens, and negative scores indicate the reverse. *SI Appendix*, Fig. S6*B* shows separation between the surface and

subterranean ecotypes, but the distribution of biphasic ecotype overlaps with both these two.

To quantify differences among ecotypes for each morphometric variable, we used generalized least-squares (GLS) and phylogenetic generalized least-squares analyses (PGLS) to conduct ANOVA and ANCOVA tests for a total of four tests. We assessed ecotype differences in Retina Total Volume, Lens Total Volume, Eye Total Volume, PC 1, PC 2, and PC 3 and applied post hoc comparisons (*SI Appendix*, Tables S5–S10). The interpretation generally did not differ whether SGL (head size) was used as a covariate (ANCOVA) or not (ANOVA). The ecotypes were easily separated based on ocular measurements. Each of the six variables showed significant differences among the ecotypes under all four analyses, except in one case. For the three raw variables, the pairwise post hoc comparisons were significant except for a few contrasts between surface and subterranean phenotypes (GLS), and surface and biphasic phenotypes (PGLS) in Lens Total Volume (*SI Appendix*, Table S7).

All PC 1 post hoc comparisons but one were significant (*SI Appendix*, Table S8). For PC 2, the GLS ANCOVA was not significant, and post hoc comparisons for the other categories of analysis were mostly significant (*SI Appendix*, Table S9). For PC 3, none of the surface–biphasic comparisons were significant (*SI Appendix*, Table S10), whereas most of the other contrasts were. Overall, the ecotypes can easily be distinguished by any of the morphometric variables, even though these phenotypes have evolved multiple times. This is easily seen, for example, in *SI Appendix*, Fig. S7, where the species are ordered by Eye Total Volume. The numerous overlapping branches indicate that the ecotypes, particularly the subterranean phenotype, do not sort out phylogenetically. To visualize the evolution of the morphometric traits on the phylogeny, we mapped Eye Total Volume, Retina Total Volume, Lens Total Volume, and SGL onto the tree under a Brownian motion model (*SI Appendix*, Figs. S8–S10). These reconstructions emphasize the multiple reductions in eye size.

Morphological and Genetic Divergence Are Uncoupled. We compared the chronogram's topology with that of a minimum evolution tree derived from a Euclidean distance matrix calculated from Retina Total Volume, Lens Total Volume, and Snout–Gular Length (*SI Appendix*, Fig. S11). The large number of crossing lines and the large normalized Robinson–Foulds distance (0.958) illustrate that the topologies are highly dissimilar. This indicates that shape evolution is largely independent of phylogeny.

Phenotypic Evolution Undergoes Rate Shifts across the Phylogeny. For Lens Total Volume, the three-rate model had the best fit to the data (AICw 0.601; *SI Appendix*, Fig. S12). For Retina Total Volume, the two-rate model was best (AICw 0.794; *SI Appendix*, Fig. S12). For Eye Total Volume, the two-rate model was best (AICw 0.513), but a combination of the two- and three-rate (AICw = 0.365) models accounted for 0.878 of the weight (*SI Appendix*, Figs. S13–S16 and Table S11). It is notable that the two-rate models of Eye Total Volume and Lens Total Volume show a drastic increase in σ^2 very near the tips of the tree. When a third rate is added to the model, there is a distinct decrease in σ^2 at the level of the ancestor of *Paedomolge* (*SI Appendix*, Fig. S12*A*). The rate shift plot of PPCI (*SI Appendix*, Fig. S16) provides a summary of the rate shifts of the eye variables. The results indicate that the factors contributing to shifts in the evolutionary rates of these traits are not specific to lineages. Specifically, the dramatic increase in σ^2 at the tips of the tree suggests recent changes in multiple lineages.

Eyes of Subterranean Species Undergo Reduction Early in Development. The structure of the retina has not been described in most of the species. The retina of surface ecotypes is composed of seven layers we identify as the retinal ganglion cell layer, inner plexiform layer, inner nuclear layer, outer plexiform layer, outer nuclear layer, photoreceptors, and pigment epithelium (*SI Appendix*, Fig. S17) (6). We identified the composite of all layers as the retina for all downstream segmentation and volume measurements of adult specimens. We also identified the ciliary body as an extension from the distal portions of the retina, attaching to the lens in adults. We assume that the ciliary body functions similarly in *Paedomolge* relative to other vertebrates, including other salamanders. In other salamanders, the ciliary body contributes to mechanically displacing the lens for accommodation. The diffusible iodine-based contrast-enhanced computed tomography (diceCT; 48) scans of early salamander development do not clearly distinguish the boundary between the posterior ciliary body and anterior retina. Therefore, we included the developing ciliary body, known as the ciliary marginal zone (49) in the retinal measurements of all early developmental stages. The lens was identified as a large spheroid cupped by the retina, and in the adults, is attached to the ciliary body. An optic nerve can be identified in all the adult and developmental specimens. It appears as a thin, relatively well-stained nerve bundle emanating from the retina.

To trace the time course of eye reduction during development, we measured the volumes of the lenses and retinae of larvae (a minimum of three individuals per stage) 1-, 2-, 3-, 4-, and 5-months postoviposition (mpo), as well as in adults (adults described above), and compared the volumes among three surface taxa (*E. nana*, *E. pterophila*–Comal Springs [CS], and *E. sosorum*) and three subterranean taxa (*E. rathbuni*, *E. latitans*–Honey Creek Cave, and *E. pterophila*–Preserve Cave [PC]) using a generalized linear model (*SI Appendix*, Table S12). ANOVA was conducted on the six species at each stage of development (*SI Appendix*, Tables S13–S18 and Fig. 2). At 2 mpo, differences emerged between ecotypes and became more striking as development continued, as illustrated in the Tukey's post hoc distribution bars and estimated marginal means (Fig. 2*A* and *SI Appendix*, Fig. S18). From stages 2 mpo to adult, Eye Total Volume varied between phenotypes, with increasingly greater eye volume in surface taxa relative to subterranean taxa (Fig. 2 *A* and *B*).

There were significant differences in volumes of the adult retinae and lenses among six species (*E. rathbuni*, *E. latitans*, *E. pterophila*–PC, *E. pterophila*–CS, *E. nana*, and *E. sosorum*) based on diceCT images (*SI Appendix*, Table S16 A–D). Total eye volume is significantly different among species ($P < 3.86e\text{-}07$, *SI Appendix*, Table S16A), and between ecotypes (Fig. 2*C*, post hoc Tukey's test; *SI Appendix*, Table S16 C and D), but not among species within ecotypes. The three subterranean species have less lens and retinal tissue than surface species. Among the subterranean species, the lens tissue volume is reduced, or in most cases absent, in adults (Fig. 1; blue versus orange circles). This is different from metamorphosed individuals outside the *Paedomolge* clade. In *Eurycea aquatica* and *Eurycea cirrigera,* the adult lens volume is greater than the retinal volume.

All subterranean adult individuals had reduced retinae and adult *E. rathbuni*, *E.* sp. 5, *E. waterlooensis*, and *Eurycea wallacei* had no lenses (Fig. 1). *E. latitans* and *E. pterophila*–PC are from polymorphic populations (i.e., populations with multiple discrete phenotypes) and have greater variation in lens development; in these populations, some individuals retained underdeveloped lenses and retinae.

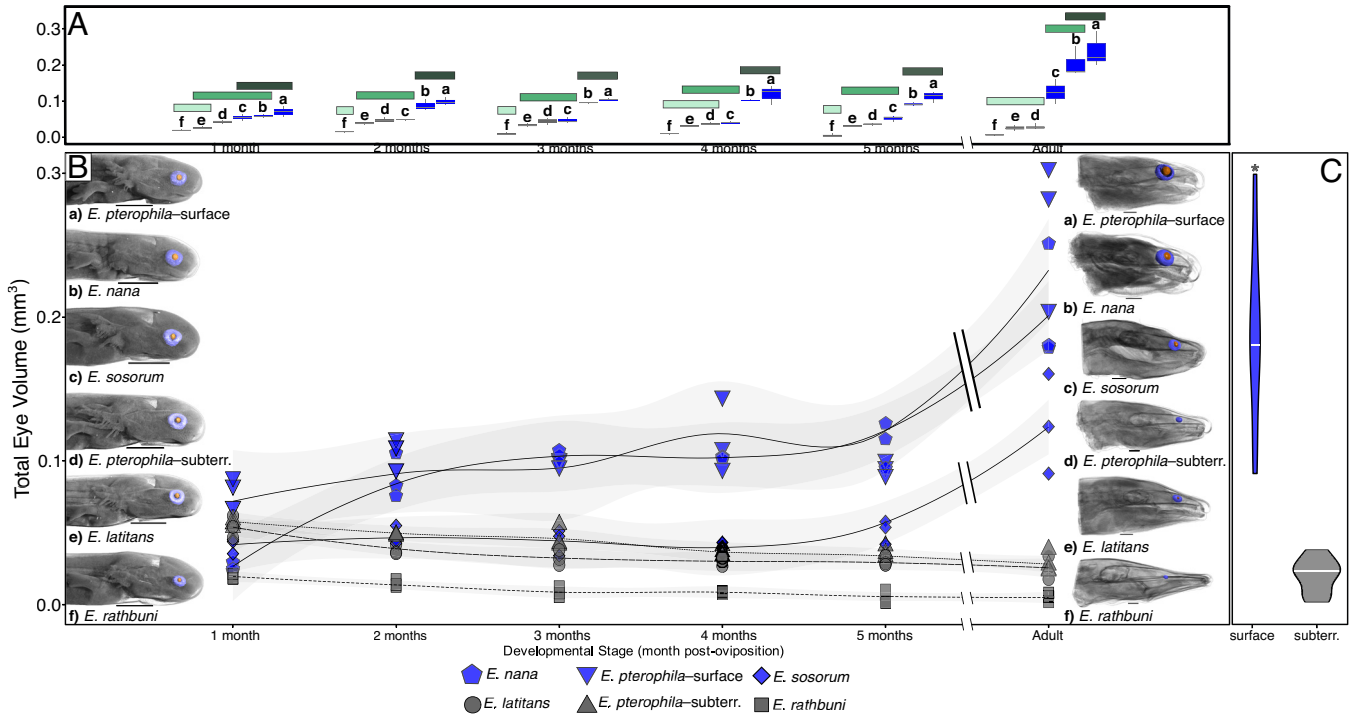

Fig. 2. (*A*) Generalized linear regression was used to measure and plot the developmental trajectories of eye volume through a developmental series of six taxa of *Eurycea* with Tukey's grouping in three shades of green and box plots associated with surface (blue) and subterranean (gray) species. Taxa include three surface populations (a: *E. pterophila*–surface; Comal Springs; b: *E. nana*; c: *E. sosorum*) and three subterranean populations (d: *E. pterophila*–subterranean; Preserve Cave; *E. latitans*; f: *E. rathbuni*). Eye volumes are plotted for each developmental stage (1 to 5 mpo and adults; n = 3 for each stage and taxon). (*B*) Standardized adult eye volumes between surface and subterranean species are significantly different (the retina in blue and lens in orange). (Scale bars indicate 1 mm.) By 1 mo of age, differences between ecotypes begin to emerge, becoming more pronounced as development progresses. Results of a generalized linear regression with adult only eye volume are shown in a violin plot in panel (*C*) with significant difference between surface (blue) and subterranean (gray) species.

PAX6 Localizes to Eyes and Neuromasts. To determine whether eye reduction in subterranean salamanders was related to diminished expression of the gene encoding the developmental transcription factor Paired-box 6 (PAX6), we compared immunolabeling for PAX6 between *E. rathbuni* and *E. nana* at 1- and 3-mpo and in adults. We examined at least 3 individuals for each species at each stage using a polyclonal anti-PAX6 antibody, validated in mammalian species and recently in *E. latitans, E. nana, and E. rathbuni* (50). Western blot analysis indicated that this antibody labeled a band at the appropriate molecular weight in tissue homogenates obtained from *E. nana* and *E. rathbuni* embryos stages 37 to 41 (*SI Appendix*, Fig. S19). We observed no statistically significant difference in PAX6 labeling in the eyes between *E. nana* and *E. rathbuni* through the two early stages of development and adults (Fig. 3). However, there is a significant difference ($P < 0.05$) in the PAX6 labeling of neuromasts between adult *E. rathbuni* and *E. nana* (Fig. 3). Specifically, *E. nana* adults showed lower levels of PAX6 labeling compared to *E. rathbuni* (Fig. 3 *B* and *G*). Moreover, we observe a negative relationship between PAX6 labeling and developmental progression in *E. nana* neuromasts relative to those of *E. rathbuni*. Labeling of this transcription factor was particularly evident in the apical appendages of the hair cells (Fig. 3 *B*–*F*).

Subterranean Species Have More Anterior Neuromasts. The observation of differences in PAX6 labeling in neuromasts of *E. rathbuni* compared to *E. nana* led us to ask whether the lateral line system of subterranean salamanders was enhanced relative to surface ecotypes. Neuromasts appear as small, round, or elliptical indentions on the skin's surface in the diceCT renderings, typically arranged in lines, matching Lannoo's description (51). To corroborate our identification of neuromasts in 1-mpo specimens, we produced a higher-resolution diceCT scan (*SI Appendix*, Fig. S1 *B* and *C*) and images using scanning electron microscopy of an adult *E. rathbuni* (Fig. 3*H*), enabling us to visualize superficial and subcutaneous structures indicative of neuromasts (52). Mapping and quantifying neuromasts of the anterior lateral line of salamanders from seven species of *Eurycea* (four surface and three subterranean species; Fig. 4) revealed a significant difference in the number of ALL neuromasts between surface and subterranean salamanders (one-way ANOVA; $F_{(6, 14)} = 16.10$, $P < 0.001$). There are significantly fewer ALL neuromasts in the four surface salamander populations than in two of the three subterranean populations ($P < 0.05$), with the increases largely explained by the addition of lines of neuromasts (Fig. 4). The remaining subterranean representative (*E. latitans* HC) did not have a significantly different number of neuromasts than surface *E. pterophila*–CS individuals ($P = 0.081$).

PCA of regional neuromast counts largely separated surface and subterranean species along PC 1, which accounted for 82.4% of the variation and had positive loadings for all neuromast counts (Fig. 4). PC 2 accounted for 11.2% of the variation and separated samples by mandibular and maxillary neuromast counts, with the greatest differences among the subterranean species (Fig. 4 and *SI Appendix*, Fig. S20). We further examined neuromast structure with scanning electron microscopy, revealing superficial structures of the neuromast, including kinocilia and stereocilia in both *E. nana* and *E. rathbuni* (*SI Appendix*, Fig. S2). Additional structures are also evident in the SEM images; for example, epidermal microvilli are visible on the surface of the skin of *E. nana* and there is a pit organ in *E. rathbuni*. Histological examination of tissue sections revealed several hallmark neuromast structures, including hair cells, mantle cells, and cilia (*SI Appendix*, Figs. S1 and S2).

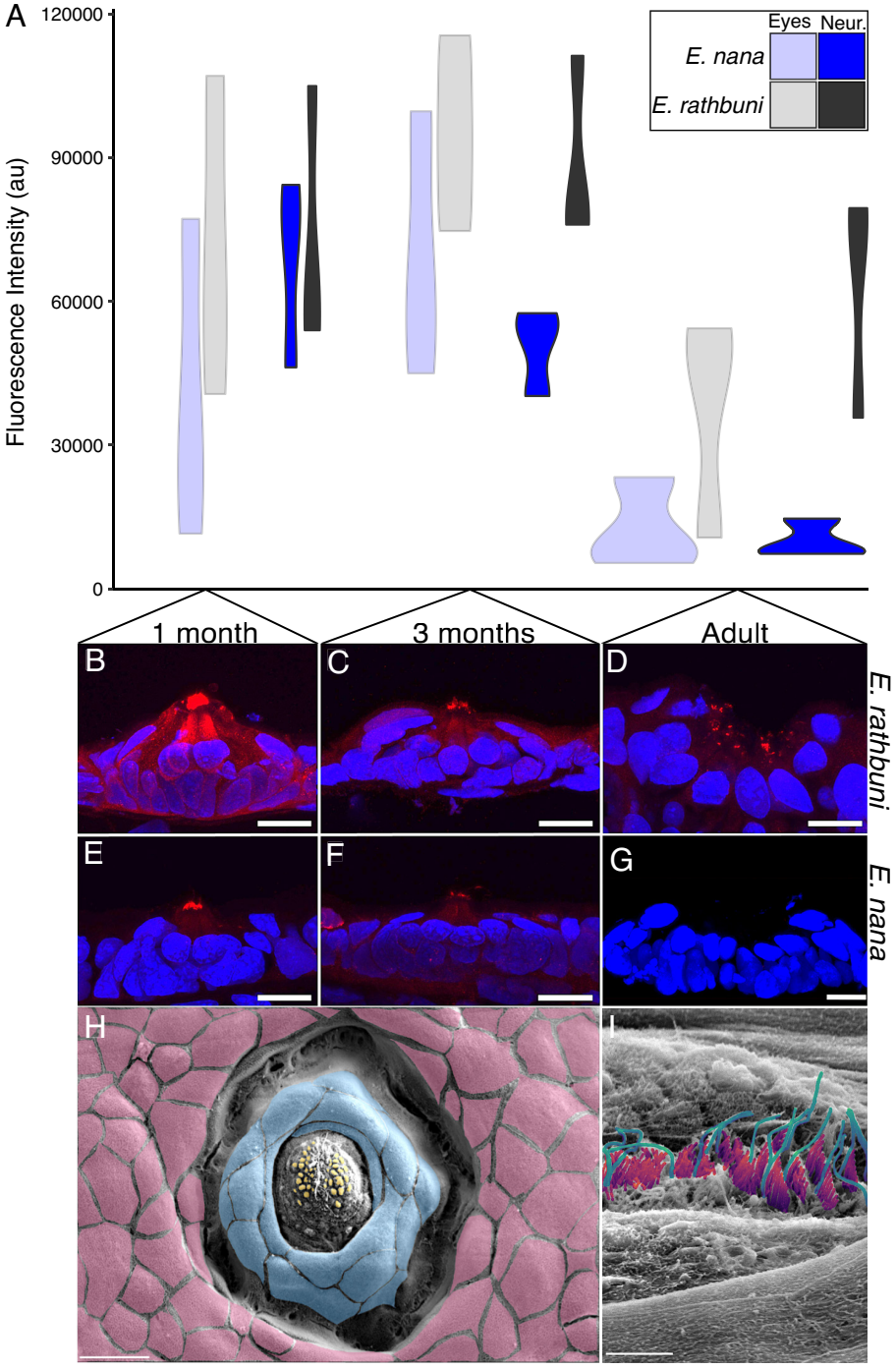

Fig. 3. Differential PAX6 labeling in eyes (Eyes; lighter colors) and neuromasts (Neur; darker colors) through ontogeny. (*A*) ANOVA point distributions show three developmental stages between two species (*E. rathbuni* in gray and *E. nana* in blue). (*B*–*G*) Sections of neuromasts labeled with DAPI nuclear stain (blue), and anti-PAX6 (red), white scale bars indicate 20 μm. An SEM image of *E. rathbuni* neuromast microstructure (*H*) identifying epithelial cells (pink), mantle cells (blue), and support cells (orange), scale bar equals 20 μm. A higher magnification of the same neuromast (*I*) shows kinocilia (aqua blue), and stereocilia (magenta), scale bar equals 5 μm.

Discussion

Repeated Eye Reduction and Cave Colonization. Our phylogenetic analysis (Fig. 1) indicates that the transition from a biphasic life history to paedomorphy occurred early in the *Paedomolge* clade, with one reversal. Invasions of subterranean environments, and the evolution of the subterranean phenotypes (including eye reduction and anterior lateral line augmentation), have occurred independently at least six times, mostly within the past few million years (Fig. 1). There have been multiple convergences and reversals in ecotypes (estimated using stochastic mapping, under any of the models).

Within a phylogenetic framework, the three ecotypes (biphasic, paedomorphic surface, and paedomorphic subterranean) are readily distinguished using the morphometric variables (either raw measures or PCs), using phylogenetically informed ANOVA and ANCOVA. Adding SGL as a covariate makes no difference, suggesting that SGL is not a good estimator of overall size. None of the continuous traits we measured were indicators of phylogenetic relationships, supporting the conclusion that eye reduction and lateral line augmentation arose independently in multiple lineages. The phylogenetic signal analysis and the cophylogenetic analysis of morphology and genetic distance support this conclusion. The rate-shift analyses suggest that some of the factors contributing to shifts in the evolutionary rates of these traits are not specific to independent lineages. Specifically, the dramatic increase in σ^2 at the tips of the tree suggests an external influence, such as the recent repeated invasion of cave habitats.

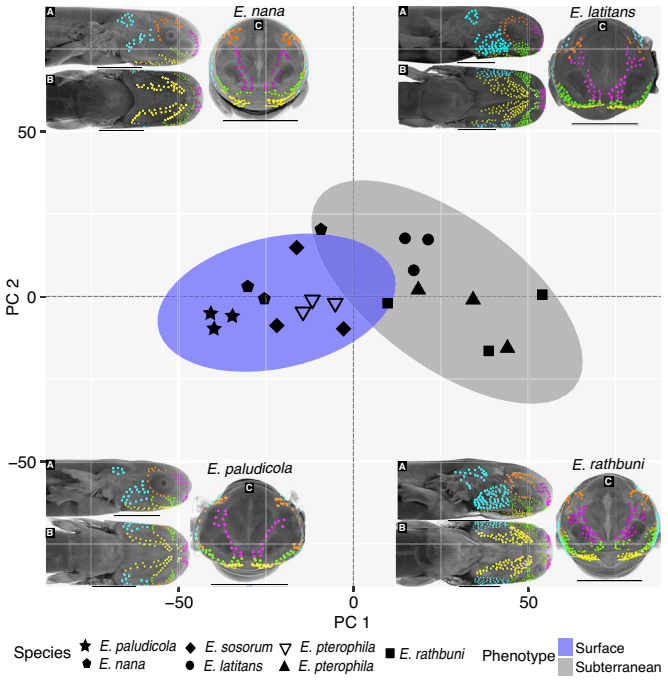

Fig. 4. PCA of neuromast counts among seven species of *Eurycea* at 1-mpo. PC 1 (positive loadings for all neuromast counts) accounts for 82.4% of the variance and indicates higher neuromast counts for subterranean compared to surface species. PC 2 accounts for 11.2% of the variance and is largely a contrast between maxillary and mandibular neuromast counts. Exemplar species and their respective neuromasts are illustrated for each quadrant of the PCA (clockwise: *E. nana*, *E. latitans*, *E. rathbuni*, and *E. paludicola*). Lateral (A), ventral (B), and frontal (C) views are shown for each exemplar species. Neuromasts are shown in situ, in postorbital (light blue), orbital (orange), mandibular (yellow), maxillary (green), and nasal (purple) regions. (Scale bars indicate 1 mm.)

Lateral Line Augmentation. In addition to eye reduction or loss, we found repeated sensory augmentation across the multiple lineages of salamanders that have independently colonized subterranean habitats. This augmentation is manifested as increased numbers of neuromasts in the anterior lateral line (ALL) system in subterranean ecotypes. We interpret the co-occurrence of eye loss and ALL enhancement as a mechanism of sensory compensation in which a reduction of a dominant sensory system led to the enhancement of another sensory system, thereby ensuring individuals retain an ability to interpret their environment.

For compensation to have occurred, the sensory modality dominant in the ancestral state must have first been diminished. Augmentation of a previously nonprimary sensory modality then occurred. This process is likely to occur following a major ecological transition in which a new environment favors one or more secondary sensory modalities (53–55). We propose that this sequence most parsimoniously describes the phenotypic transition exemplified by cave-dwelling salamanders. Namely, vision is important in feeding, navigating, and finding mates in surface salamanders (56), which is suggested by the photic environment and ancestral presence of well-developed eyes for *Eurycea*. Reliance on light becomes impossible underground, irrespective of whether eye loss occurs immediately upon habitat transition. This reduced ability to use vision to interact with the environment may facilitate an alternative sensory system to become dominant. For aquatic animals, it is common to evolve or augment mechanosensory systems capable of sensing (57, 58), interpreting (59, 60), and mapping changes in water pressure (61). Such augmentation is exemplified by distantly related groups with convergent mechanoreceptor systems such as the neuromasts of fishes (36, 37), the dome pressure receptors of crocodilians (62), and the vibrissae of aquatic mammals (63).

We found that numbers of neuromasts increased on the head, mandibular, maxillary, postorbital, and nasal regions (Fig. 4 and *SI Appendix*, Fig. S20). The increase in postorbital neuromasts may provide enhanced sensory capability by extending coverage of the posterior region of the head, especially considering the expanded surface area offered by dorsoventral compression and lateral expansion of the heads of most subterranean species (19). An increase in neuromasts posterior to the eye may assist in predator avoidance or mating. Like the mandibular, maxillary, and postorbital regions, the nasal and orbital regions show increased neuromast counts in subterranean species, but to a lesser degree. Maxillary and mandibular concentrations presumably facilitate prey detection in an austere subterranean environment. The vibrations released by potential prey items (isopods, amphipods, and other invertebrates) are signals readily interpreted by neuromasts (64). Chemosensory organs could also be important in this regard.

We show that a pronounced reduction in ocular development correlates with increased neuromast counts in subterranean salamander lineages. Thus, the augmentation in neuromast numbers among subterranean salamanders provides an enhanced sensory modality compared to the ancestral condition. Sensory compensation could be accomplished through paedomorphy. Mid-Miocene climatic warming and associated aridification in Texas presumably favored a transition to paedomorphy in the ancestor of *Paedomolge* (17, 26). The descendant species in this group are obligately aquatic and retain larval characteristics (e.g., gills and tail fin) adaptive for an aquatic life history, except in rare instances in one population of one species (*E. troglodytes*).

Role of Heterochrony. Heterochrony—the displacement of a trait's development in time relative to its ancestral state—likely played an important role in trait transitions from surface to subterranean phenotypes. However, the molecular mechanisms that produce paedomorphic and peramorphic (i.e., overdevelopment of a trait in derived adults; 65, 66) traits are poorly understood. Furthermore, paedomorphy could be manifested to different degrees. For example, the failure of eye development may reflect a form of paedomorphosis in which gonadal maturation occurs while other aspects of the body retain a juvenile state or, in this case of the eye, possibly an embryonic state.

Similarly, paedomorphy may also play a role in enhanced lateral line development. Although the lateral line system is absent in most tetrapods, it is present in larval amphibians and in salamanders that retain an aquatic larval morphology into adulthood, such as *Ambystoma mexicanum* (67). In contrast, terrestrial paedomorphic salamanders, such as many bolitoglossines with direct development, do not possess a lateral line system. In many biphasic salamanders, the anatomical distribution and arrangement of the lateral line changes after metamorphosis, and neuromasts are lost altogether in some direct-developing salamander species (e.g., *Desmognathus aeneus* and *D. wrighti*; 68). However, the harbingers of neuromast development—afferent lateral line neurons—are still present in these *Desmognathus* species, suggesting a degree of neuro-anatomical paedomorphy (69). Interestingly, facultative metamorphosis occurs in at least two species within *Paedomolge* (*E. troglodytes* and *E.* sp. 3), and our observation of facultative metamorphosis in *E.* sp. 3 is shown in Fig. 1.

Surface paedomorphic salamanders have a suite of characteristics that are often associated with surface-dwelling organisms, including pigmentation, relatively small and robust limbs, and fully developed eyes (6, 23, 25). We observed lenses, well-developed retinae, and optic nerves in all surface-dwelling species. Furthermore, the lens and retina of surface species are markedly larger than those observed in subterranean *Eurycea* (Fig. 1). Most obligately

subterranean *Eurycea*, such as *E. rathbuni* and *E. wallacei* (70), have drastically reduced eyes (Fig. 1), a characteristic that reflects subterranean-adapted morphology and which is observed in other subterranean salamanders (e.g., *E. spelaea* and *Proteus anguinus*; 30, 31, 71, 72), subterranean fishes (e.g., *A. mexicanus*, *Phreatichthys andruzzii*, *Sinocyclocheilus anophthalmus,* and *Pimelodella kronei*; 7, 73–75), fossorial organisms (e.g., moles and snakes; 76–78), as well as invertebrates (79, 80). Furthermore, a number of *Eurycea* species (*E. rathbuni*, *E.* sp. 4, E. sp. 5, *E. waterlooensis*, *E. troglodytes*, and *E. wallacei*) exhibit a few vestigial retinal layers surrounded by pigment epithelium (Fig. 1) (6, 29, 41, 81). Pigmentation surrounding the eye suggests light would be unable to pass through choroidal pigment or pigment epithelium to be absorbed by any existing photoreceptors, a finding suggested for *E. rathbuni* (6) and *P. anguinus* (82). Interestingly, the optic nerve is retained in both species, suggesting a possible sensory, but not necessarily image-forming, function (69).

Role of *pax6*. Paired-box 6 gene (*pax6*) controls eye development across vertebrates (81–83), as does its homolog (*eyeless*) in invertebrates (84, 85). The product of this gene, PAX6, is a well-known transcription factor and is often observed as an endonucleic protein that plays a critical spatiotemporal role throughout development (86–88). Interestingly, PAX6 has also been documented in tissues other than eyes, transiently through development (89–91), in cell culture (92), and during regeneration (93, 94). Extensive work by Jeffery (5) compared eye development between surface and subterranean phenotypes of *A. mexicanus*; he showed that the overexpression of *shh* down the midline of the subterranean tetra leads to the downregulation of *pax6* (7). This downregulation results in apoptosis and underdeveloped eyes in subterranean *A. mexicanus*, and a similar trend has been noted in the eye of *E. rathbuni* (6). Here, we expand sample size and add later developmental stages. We found labeling in the developing eye tissue of *E. rathbuni* is not significantly different from that of *E. nana* through ontogeny (Fig. 3). This finding aligns more closely with observations in another cavefish species (*Phreatichthys andruzzii*), in which the expression of *pax6* during early development does not deviate from canonical expression, suggesting that an alternative molecular target, and not primarily PAX6, is responsible for eye reduction (95, 96).

In contrast to the observations in *Astyanax* (7), we did not observe significantly different labeling of PAX6 through development in eyes of *Eurycea*. Instead, we found PAX6 labeling waned through development in the neuromasts of *E. nana,* resulting in a declining trend through the three stages. We recently reported our observation of PAX6-labeling in the neuromast of *E. rathbuni* and *E. nana* (50), and here expand those observations by quantifying the labeling of PAX6 in the neuromasts of the subterranean *E. rathbuni* and surface *E. nana* through three developmental stages. Whether the persistence of PAX6 labeling in *E. rathbuni* neuromasts is a result of their augmentation requires further testing; however, an increase in the number of ALL neuromasts was evident in all the subterranean forms (*E. rathbuni*, *E. latitans*–HC, and *E. pterophila*–PC) we examined. Likewise, the subterranean populations of dimorphic species (*E. latitans* and *E. pterophila*–PC) have more neuromasts (Fig. 4), as do some subterranean populations of *A. mexicanus* (7).

Materials and Methods

Sample Collection and Sequencing. Salamanders were either collected from the wild or donated by the San Marcos Aquatic Resources Center (SMARC), USFWS, San Marcos, TX (*E. nana, E. pterophila*–CS, *E. rathbuni,* and *E. sosorum*), and the City of Austin (*E. sosorum and E. waterlooensis*). We assembled a dataset of 26 cytochrome b (*cytb*) sequences and 17 recombination activating gene 1 (*rag1*) from published GenBank sequences (n = 22) and sequences that we generated (n = 4; Fig. 1 and *SI Appendix*, Table S19). We isolated DNA using spin column kits (Qiagen) and amplified a fragment of *cytb* (17). Sanger sequencing was performed by Eton Bioscience, Inc., using the same primers that were used in PCR. Geneious Prime 2024.0.3 (GraphPad Software, LLC) was used to assemble forward and reverse sequences and aligned using MAFFT 4.475 (97); bases with more than a 1% chance of an error were trimmed from the sequence ends (*SI Appendix*, Table S19).

Phylogenetic and Comparative Analyses. We performed a maximum likelihood phylogenetic analysis using IQ-TREE 2.3.4 (98) with 10 replicates under the edge-proportional partition model (99) with 100,000 ultrafast bootstrap replicates (100, 101) to assess support (*SI Appendix*, Tables S9 and S10). Each analysis was repeated 10 times to ensure consistency. All currently known species of *Paedomolge* were included. The phylogram was converted to a chronogram with a tip to root distance of 1.0 using the R function *ape::chronos()*.

Because some of the species were polymorphic for ecotype (particularly, species with some surface populations and subterranean populations), we included one representative of each ecotype in the phylogenetic analysis, even though there may be multiple ecotypes within a species. This yields a conservative estimate of the number of state changes.

Ancestral state reconstruction on both continuous and discrete traits was performed using the R packages *ape version 5.8* (102) and *phytools* version 2.3-0 (103). For details of the models, see the *SI Appendix*.

Stochastic Character Mapping. To quantify the frequency of character-state changes, stochastic character mapping (45), a Markov Chain Monte Carlo procedure that simulates a phylogenetic map of history of a discrete character under a specified model, was performed using *phytools::make.simmap()*. We analyzed the ecotype data under four Mk models and four corresponding Mk gamma models; the latter include a rate heterogeneity parameter. We excluded *E. wallacei* because other *Eurycea* species in this region of the phylogeny are poorly sampled, and inclusion of extreme values of *E. wallacei* appeared to bias the trait estimates. Additional details are given in *SI Appendix*.

Shape Differences among Ecotypes. Principal component analyses were performed on the species means of the untransformed variables Retina Total Volume, Lens Total Volume, and Snout-Gular Length. Standard (PCA, nonphylogenetic) analyses were performed using the *stats::prcomp()* with a correlation matrix. PPCA were performed using *phytools::phyl.pca()*. Results are in *SI Appendix*, Fig. S6.

The *nlme::gls()* function was used to perform GLS and PGLS analyses under ANOVA and ANCOVA (SGL as the covariate) models, for a total of four tests for each variable. Life History was the predictor. The *ape::corbrownian()* function was used to specify within-group phylogenetic correlation structure for the PGLS analyses. We assessed ecotype (life history) differences in Retina Volume, Lens Volume, Eye Total Volume, PC 1, PC 2, and PC 3) and applied post hoc comparisons using *multicom::glht()* and the "Tukey" option (*SI Appendix*, Tables S5–S10).

Phylogenetic Signal. The amount of phylogenetic signal (lambda) in the continuous traits was estimated using *phytools::phylosig()* (47, 103). The continuous variables were mapped onto the chronogram under the Brownian motion model using *phytools::contMap()*. The maps for all continuous variables are shown in the *SI Appendix*, Figs. S8–S10.

Chronogram. Raw values (mm^3) for Eye Total volume by species (y-axis) were plotted against scaled genetic divergence (x-axis) and superimposed on the chronogram, using *phytools::phenogram()*.

Rate-Shift Analyses. The rate-shift analyses (103) estimated points in time on the chronogram where the rate of character change, as measured by σ^2 (evolutionary rate under Brownian motion) has shifted across all lineages simultaneously rather than along one branch. The algorithm identifies optima for one, two, three, etc., points, at which there is a shift in the value of σ^2. These shift points delimit so-called regimes, the slices of time during which the σ^2 is constant. We analyzed each variable for four regimes and used AIC weight to determine the best-fit model.

Cophylogenetic Analysis of Morphology and Genetic Divergence. This analysis compares two trees, the DNA chronogram used for other analyses, and a phenotypic Minimum Evolution tree [*ape::fastme.bal()*; (104)] calculated from a standardized Euclidean distance matrix (*factoextra::get_dist()*). Three variables were used: Retina Total Volume, Lens Total Volume, and Snout-Gular Length (SGL). The normalized Robinson–Foulds distance, which describes similarity of the topologies, was calculated using *phangorn::RF.dist()*. The distance ranges from 0 to 1; the calculated distance (0.958) means that the topologies are very different. The diagram was produced by the *phytools::cophylo()* function.

PAX6 Immunohistochemistry and Imaging. Specimens were euthanized and followed The University of Texas at Austin Institutional Animal Care and Use Committee protocol AUP-2021-00090, fixed in 4% paraformaldehyde, cryoprotected, embedded, and sectioned at 15 μm using a Cryostat. Sections were blocked, then incubated with anti-PAX6 antibody, followed by a secondary antibody (1:500), and mounted. Imaging was performed with standardized laser settings. PAX6 fluorescence intensity in neuromast mantle cells was quantified using Olympus's Fluoview tool, averaging values from three neuromasts per individual, while negative controls provided a reference but were excluded from statistical analysis. See *SI Appendix, Methods* for more detail.

Specimens.

Early development. All animal manipulations were approved by The University of Texas at Austin Institutional Animal Care and Use Committee under AUP-2021-00090. A developmental series was collected for four species, representing one subterranean species (*E. rathbuni*) and three surface species, *E. nana*, *E. sosorum*, and *E. pterophila*–CS. Three individuals representing the above species for each stage were collected from the SMARC, TX, United States Fish and Wildlife Service (USFWS), and incubated in an environmental chamber at 21.1 °C until they were euthanized using 0.2% MS222. A developmental series was obtained for two additional species and one population representing the subterranean phenotype of *E. pterophila*–PC. These three species were collected from in-house breeding populations at The University of Texas at Austin, maintained, and euthanized as described above. Three individuals for each species or population at each stage were collected. In total, a developmental series for six lineages of Texas *Euyrcea* were collected including both forms (surface and subterranean) of a polymorphic species (*E. pterophila*) resulting in 108 specimens. Staging was determined by morphology (105), and embryos were maintained at constant temperature with no lighting except when fed by hand once yolk was fully absorbed after 2 mpo. Light exposure during feeding was estimated to be approximately 10 to 15 min, twice a week. All specimens were collected and transported under Texas Parks and Wildlife scientific permit number SPR-0119-004, and State Park permit number 57-22.

Adult specimens. Adult salamanders of fourteen species were collected including *E. rathbuni* (n = 3), *E. nana* (3), *E. sosorum* (3), *E. pterophila*–PC (3), *E. latitans* from Honey Creek Cave (n = 3), *E. latitans* from Honey Creek State Natural Area (3), *E. pterophila*–CS (3), *E. neotenes* (3), *E. troglodytes* (1), *E. waterlooensis* (n = 1), *E. naufragia* (n = 1), *E. tonkawae* from Testudo Tube (n = 1), *E. tonkawae* from Bull Creek (n = 1), *E. chisholmensis* (n = 1), *E.* sp. 5 from Jacob's Spring (n = 1), *E.* sp. 4 from New Braunfels well (n = 3), and *E.* sp. 1, 2, and 3 as identified in ref. 25 (n = 1 each). We recognize the relatively low support for the genetic distinctiveness of three species (*E. neotenes*, *E. latitans*, and *E. pterophila*), and there is ongoing work to resolve this (106). However, the focus of this manuscript is not to determine taxonomic status; therefore, we adopt the current taxonomy (25). Salamanders were euthanized using 0.2% MS222 and decapitated in preparation for fixation and diceCT scanning.

We examined eyes from adults of six species (*E. nana*, *E. sosorum*, *E. pterophila*–CS, *E. pterophila*–PC, *E. latitans*, and *E. rathbuni*) using diffusible iodine-based contrast-enhanced computed tomography (diceCT; *SI Appendix, Methods*, 48, 107) and optimized at reconstruction (*SI Appendix, Methods*, 108) to reveal soft tissues. We divided our sample into two ecotypes. Three species (*E. latitans, E. rathbuni,* and *E. pterophila*–PC) exhibit subterranean morphology, and three (*E. nana, E. sosorum*, and *E. pterophila*–CS) exhibit surface morphology. We took the relative eye volume (mm^2) by measuring total volume of functional eye tissue, defined as the sum of lens and retina volumes, and standardized by gular fold to snout length (GFL). We performed a generalized linear model ANOVA and Tukey's post hoc test in R (109) for each developmental stage from 1 to 5 mpo and adult for five species, one of which was represented by two ecotypes. Details of fixation, staining, and CT Scanning, rendering, segmentation, and immunohistochemistry are presented in *SI Appendix, Methods*.

Data, Materials, and Software Availability. DNA sequences data have been deposited in GenBank. All accession numbers are listed in *SI Appendix*, Table S19 (21). All other data are included in the manuscript and/or *SI Appendix*.

ACKNOWLEDGMENTS. We thank Katie Bockrath, David Britton, Desiree More, Braden West, Justin Crow, Adam Daw, and other staff of the San Marcos Aquatic Resources Center, USFWS, for providing the salamander larvae that made much of this work possible. We also thank Debbie and Don Davis, Ryan Hoffman, Zach Adcock, Pete Diaz, The Bexar Grotto Group, Staff at Guadalupe River State Park, Honey Creek State Natural Area, and Lost Maples State Natural Area, Dee Ann Chamberlain, Rustin Tabor, James Peterson, Jacob Owen, Marco Jones, and Shannon Carrasco for assistance with site access and collecting; core facility staff Jessie Maisano, Matthew Colbert, David Edey, Alissa Savage, Jacob Bisbal, and Jacob Armitage for training and guidance; Guillaume Dury for help with navigating Inkscape and constructive critique of the figures through several iterations; Christian Teague for help with westerns; and Liam Revell for modifying his phytools package for our use. The equipment in The Analysis Research Service Center is supported by funds from the Materials Applications Research Center of Texas State University. This work was supported by the University of Arizona Department of Cellular and Molecular Medicine and the NSF supported this work (award DEB2032632 to D.M.H. and T.J.D.; DEB203263 to D.M.G.); NSF had no involvement in the conduct of the study, preparation of the manuscript, or decision to submit it for publication.

Author affiliations: [a]Department of Integrative Biology and Biodiversity Center, The University of Texas at Austin, Austin, TX 78712; [b]Department of Biology, Texas State University, San Marcos, TX 78666; and [c]Department of Cellular and Molecular Medicine, University of Arizona College of Medicine, Tucson, AZ 85724

Author contributions: R.U.T., T.J.D., D.M.G., and D.M.H. designed research; R.U.T., B.A.D., N.R.H., S.L., and T.J.D. performed research; R.U.T., T.J.D., D.M.G., P.M.G., and D.M.H. contributed new reagents/analytic tools; R.U.T., B.A.D., N.R.H., S.L., T.J.D., D.M.G., P.M.G., D.C.C., and D.M.H. analyzed data; and R.U.T., D.C.C., and D.M.H. wrote the paper.

1. S. Rétaux, D. Casane, Evolution of eye development in the darkness of caves: Adaptation, drift, or both? *Evodevo* **4**, 26 (2013).
2. D. Soares, M. L. Niemiller, Extreme adaptation in caves. *Anat. Rec.* **303**, 15–23 (2020).
3. D. Culver, B. Sket, Hotspots of subterranean biodiversity in caves and wells. *J. Cave Karst Stud.* **62**, 11–17 (2000).
4. Š Gorički, M. Niemiller, D. Fenolio, "Salamanders" in *Encyclopedia of Caves*, W. B. White, D. C. Culver, Eds. (Academic Press, Elsevier, 2012), pp. 665–676.
5. W. R. Jeffery, Adaptive evolution of eye degeneration in the Mexican blind cavefish. *J. Hered.* **96**, 185–196 (2005).
6. R. U. Tovar *et al.*, Comparative development and ocular histology between epigean and subterranean salamanders (*Eurycea*) from central Texas. *PeerJ* **9**, e11840 (2021).
7. W. R. Jeffery, Evolution and development in the cavefish *Astyanax*. *Curr. Top. Dev. Biol.* **86**, 191–221 (2009).
8. M. E. Protas *et al.*, Genetic analysis of cavefish reveals molecular convergence in the evolution of albinism. *Nat. Genet.* **38**, 107–111 (2006).
9. D. Schluter, Adaptive radiation along genetic lines of least resistance. *Evolution* **50**, 1766–1774 (1996).
10. D. I. Bolnick, R. D. H. Barrett, K. B. Oke, D. J. Rennison, Y. E. Stuart, (Non)parallel evolution. *Annu. Rev. Ecol. Evol. Syst.* **49**, 303–330 (2018).
11. W. R. Jeffery, *Astyanax* surface and cave fish morphs. *EvoDevo* **11**, 14 (2020).
12. J. Krishnan, N. Rohner, Cavefish and the basis for eye loss. *Philos. Trans. R. Soc. B Biol. Sci.* **372**, 20150487 (2017).
13. M. L. D. Worsham, A. Bond, J. R. Gibson, D. G. Huffman, Biogeography of selected spring endemics in Texas interglacial-drought refugia with unexpected insights from a spring-dependent nematode parasite. *Hydrobiologia* **2**, 97–133 (2023).
14. P. Chakrabarty, J. Prejean, M. Niemiller, The Hoosier cavefish, a new and endangered species (Amblyopsidae, Amblyopsis) from the caves of southern Indiana. *ZooKeys* **412**, 41–57 (2014).
15. G. Longley, The Edwards Aquifer: Earth's most diverse groundwater ecosystem? *Int. J. Speleol.* **11**, 123–128 (1981).
16. C. R. Maupin *et al.*, Abrupt Southern Great Plains thunderstorm shifts linked to glacial climate variability. *Nat. Geosci.* **14**, 396–401 (2021).
17. D. M. Hillis, D. A. Chamberlain, T. P. Wilcox, P. T. Chippindale, A new species of subterranean blind salamander (Plethodontidae: Hemidactyliini: Eurycea: Typhlomolge) from Austin, Texas, and a systematic revision of central Texas paedomorphic salamanders. *Herpetologica* **57**, 266–280 (2001).
18. J. J. Wiens, P. T. Chippindale, D. M. Hillis, When are phylogenetic analyses misled by convergence? A case study in Texas cave salamanders. *Syst. Biol.* **52**, 501–514 (2003).
19. S. S. Sweet, Secondary contact and hybridization in the Texas cave salamanders *Eurycea neotenes* and *E. tridentifera*. *Copeia* **1984**, 428–441 (1984).

20. L. Stejneger, Description of a new genus and species of blind tailed batrachians from the subterranean waters of Texas. *Proc. U.S. Natl. Mus.* **18**, 619–621 (1896).
21. R. U. Tovar *et al.*, DNA sequence alignment for phylogenetic analysis. Texas Data Depository. https://dataverse.tdl.org/dataset.xhtml?persistentId=doi:10.18738/T8/6LK0WJ. Deposited 20 May 2025.
22. W. R. Jeffery *et al.*, Cavefish as biological models in the laboratory and in the wild. *Zool. Res.* **44**, 834–836 (2023).
23. N. F. Bendik, J. M. Meik, A. G. Gluesenkamp, C. E. Roelke, P. T. Chippindale, Biogeography, phylogeny, and morphological evolution of central Texas cave and spring salamanders. *BMC Evol. Biol.* **13**, 201 (2013).
24. P. Chippindale, A. H. Price, J. J. Wiens, D. M. Hillis, Phylogenetic relationships and systematic revision of central Texas hemidactyliine plethodontid salamanders. *Herpetol. Monogr.* **14**, 1–80 (2000).
25. T. J. Devitt, A. M. Wright, D. C. Cannatella, D. M. Hillis, Species delimitation in endangered groundwater salamanders: Implications for aquifer management and biodiversity conservation. *Proc. Natl. Acad. Sci. U.S.A.* **116**, 2624–2633 (2019).
26. P. Chippindale, A. Price, D. Hillis, A new species of perennibranchiate salamander (*Eurycea*: Plethodontidae) from Austin, Texas. *Herpetologica* **49**, 248–259 (1993).
27. G. Schlosser, Induction and specification of cranial placodes. *Dev. Biol.* **294**, 303–351 (2006).
28. K. V. Fite, W. F. Blair, *The Amphibian Visual System: A Multidisciplinary Approach* (Academic Press, 1976).
29. C. H. Eigenmann, The eyes of the blind vertebrates of North America, II. The eyes of *Typhomolge rathbuni* Stejneger. *Trans. Am. Microsc. Soc.* **21**, 49–60 (1900).
30. A. Möller, Die struktur des auges bei Urodelen verschiedener Körpergröße. *Zool. Jahrb. Abt. Allg. Zool. Physiol. Tiere.* **62**, 138–182 (1951).
31. J. P. Durand, Ocular development and involution in the European cave salamander. *Proteus anguinus* Laurenti. *Biol. Bull.* **151**, 450–466 (1976).
32. C. A. Emerling, M. S. Springer, Eyes underground: Regression of visual protein networks in subterranean mammals. *Mol. Phylogenet. Evol.* **78**, 260–270 (2014).
33. N. Rohner *et al.*, Cryptic variation in morphological evolution: Hsp90 as a capacitor for loss of eyes in cavefish. *Science* **342**, 1372–1375 (2013).
34. B. Chen *et al.*, Sensory evolution in a cavefish radiation: Patterns of neuromast distribution and associated behaviour in *Sinocyclocheilus* (Cypriniformes: Cyprinidae). *Proc. R. Soc. B Biol. Sci.* **289**, 20221641 (2022).
35. S. Turk, B. Sket, Ş Sarbu, Comparison between some epigean and hypogean populations of *Asellus aquaticus* (Crustacea: Isopoda: Asellidae). *Hydrobiologia* **337**, 161–170 (1996).
36. C. V. H. Baker, M. S. Modrell, J. A. Gillis, The evolution and development of vertebrate lateral line electroreceptors. *J. Exp. Biol.* **216**, 2515–2522 (2013).
37. R. Rodríguez–Morales, Sensing in the dark: Constructive evolution of the lateral line system in blind populations of *Astyanax mexicanus*. *Ecol. Evol.* **14**, e11286 (2024).
38. M. Yoshizawa, W. R. Jeffery, S. M. van Netten, M. J. McHenry, The sensitivity of lateral line receptors and their role in the behavior of *Astyanax mexicanus*. *J. Exp. Biol.* **217**, 886–895 (2014).
39. T. Teyke, Morphological differences in neuromasts of the blind cave fish *Astyanax hubbsi* and the sighted river fish *Astyanax mexicanus*. *Brain Behav. Evol.* **35**, 23–30 (1990).
40. R. G. Northcutt, H. Bleckmann, Pit organs in axolotls: A second class of lateral line neuromasts. *J. Comp. Physiol. A* **172**, 439–46 (1993).
41. G. Roth, Visual Behavior in Salamanders (Springer-Verlag Berlin Heidelberg, Germany, 1987), pp. 89–128.
42. A. A. Stewart, J. J. Wiens, A time-calibrated salamander phylogeny including 765 species and 503 genes. *Mol. Phylogenet. Evol.* **204**, 108272 (2024).
43. P. O. Lewis, A likelihood approach to estimating phylogeny from discrete morphological character data. *Syst. Biol.* **50**, 913–925 (2001).
44. K. P. Burnham, D. R. Anderson, Multimodel inference: Understanding AIC and BIC in model selection. *Sociol. Methods Res.* **33**, 261–304 (2004).
45. J. P. Huelsenbeck, R. Nielsen, J. P. Bollback, Stochastic mapping of morphological characters. *Syst. Biol.* **52**, 131–158 (2003).
46. M. Pagel, Inferring the historical patterns of biological evolution. *Nature* **401**, 877–884 (1999).
47. L. J. Revell, L. J. Harmon, *Phylogenetic Comparative Methods in R* (Princeton University Press, 2022).
48. P. M. Gignac *et al.*, Diffusible iodine-based contrast-enhanced computed tomography (diceCT): An emerging tool for rapid, high-resolution, 3-D imaging of metazoan soft tissues. *J. Anat.* **228**, 889–909 (2016).
49. A. J. Fischer, J. L. Bosse, H. M. El-Hodiri, The ciliary marginal zone (CMZ) in development and regeneration of the vertebrate eye. *Exp. Eye Res.* **116**, 199–204 (2013).
50. B. A. Dobbins *et al.*, PAX6 protein in neuromasts of the lateral line system of salamanders (*Eurycea*). *PLoS One* **19**, e0293163 (2024).
51. M. J. Lannoo, Neuromast topography in urodele amphibians. *J. Morphol.* **191**, 247–263 (1987).
52. C. Hong, H. Shi-Qiang, H. Heatwole, Ampullary organs, pit organs, and neuromasts of the Chinese giant salamander, *Andrias davidianus*. *J. Morphol.* **226**, 149–157 (1995).
53. I. W. Keesey *et al.*, Inverse resource allocation between vision and olfaction across the genus *Drosophila*. *Nat. Commun.* **10**, 1162 (2019).
54. M. S. Kabir, R. Venkatesan, M. Thaker, Multiple sensory modalities in diurnal geckos are associated with the signaling environment and evolutionary constraints. *Integr. Org. Biol.* **2**, obaa027 (2020).
55. J. Wu, H. Jiao, N. B. Simmons, Q. Lu, H. Zhao, Testing the sensory trade-off hypothesis in New World bats. *Proc. R. Soc. B Biol. Sci.* **285**, 20181523 (2018).
56. D. B. Wake, S. M. Deban, "Terrestrial feeding in salamanders" in *Feeding: Form, Function, Phylogeny*, K. Schwenk, Ed. (Academic Press, 2000), pp. 95–116.
57. R. Weissert, C. von Campenhausen, Discrimination between stationary objects by the blind cave fish *Anoptichthys jordani* (Characidae). *J. Comp. Physiol.* **143**, 375–381 (1981).
58. E. T. Lunsford, A. Paz, A. C. Keene, J. C. Liao, Evolutionary convergence of a neural mechanism in the cavefish lateral line system. *Elife* **11**, e77387 (2022).
59. L. Espinasa, R. Diamant, E. Vinepinsky, M. Espinasa, Evolutionary modifications of *Astyanax* larval prey capture (LPC) in a dark environment. *Zool. Res.* **44**, 750–760 (2023).
60. D. E. Edgley, M. J. Genner, Adaptive diversification of the lateral line system during cichlid fish radiation. *iScience* **16**, 1–11 (2019).
61. S. Coombs, R. A. Conley, Dipole source localization by the mottled sculpin II. The role of lateral line excitation patterns. *J. Comp. Physiol. [A]* **180**, 401–415 (1997).
62. D. Soares, Neurology: An ancient sensory organ in crocodilians. *Nature* **417**, 241–242 (2002).
63. B. L. Boublil, C. A. Diebold, C. F. Moss, Mechanosensory hairs and hair-like structures in the animal kingdom: Specializations and shared functions serve to inspire technology applications. *Sensors (Basel)* **21**, 6375 (2021).
64. M. Yoshizawa, Š Gorički, D. Soares, W. R. Jeffery, Evolution of a behavioral shift mediated by superficial neuromasts helps cavefish find food in darkness. *Curr. Biol.* **20**, 1631–1636 (2010).
65. P. Alberch, S. J. Gould, G. F. Oster, D. B. Wake, Size and shape in ontogeny and phylogeny. *Paleobiology* **5**, 296–317 (1979).
66. K. J. McNamara, Heterochrony: The evolution of development. *Evol. Educ. Outreach.* **5**, 203–218 (2012).
67. R. G. Northcutt, K. Brändle, B. Fritzsch, Electroreceptors and mechanosensory lateral line organs arise from single placodes in axolotls. *Dev. Biol.* **168**, 358–373 (1995).
68. D. B. Wake, G. Roth, K. C. Nishikawa, The fate of the lateral line system in plethodontid salamanders. *Am. Zool.* **27**, 166A (1987).
69. G. Roth, K. C. Nishikawa, C. Naujoks-Manteuffel, A. Schmidt, D. B. Wake, Paedomorphosis and simplification in the nervous system of salamanders. *Brain Behav. Evol.* **42**, 137–170 (1993).
70. R. A. Brandon, Structure of the eye of *Haideotriton wallacei*, a North American troglobitic salamander. *J. Morphol.* **124**, 345–352 (1968).
71. C. H. Eigenmann, W. A. Denny, The eyes of the blind vertebrates of North America, III: The structure and ontogenic degeneration of the eyes of the Missouri cave salamander, an account based on material collected with a grant from The Elizabeth Thomson Science Fund. *Biol. Bull.* **2**, 33–41 (1900).
72. M. Tesařová *et al.*, Living in darkness: Exploring adaptation of *Proteus anguinus* in 3 dimensions by X-ray imaging. *Gigascience* **11**, giac030 (2022).
73. R. Berti *et al.*, Eye degeneration in the blind cave-dwelling fish *Phreatichthys andruzzii*. *Can. J. Zool.* **79**, 1278–1285 (2001).
74. E. Trajano, Diversity of Brazilian troglobitic fishes: Models of colonization and differentiation in subterranean habitats. *Diversity* **13**, 106 (2021).
75. F. Meng *et al.*, Evolution of the eye transcriptome under constant darkness in *Sinocyclocheilus* cavefish. *Mol. Biol. Evol.* **30**, 1527–1543 (2013).
76. B. F. Simões *et al.*, Visual system evolution and the nature of the ancestral snake. *J. Evol. Biol.* **28**, 1309–1320 (2015).
77. F. D. Carmona, R. Jiménez, J. M. Collinson, The molecular basis of defective lens development in the Iberian mole. *BMC Biol.* **6**, 44 (2008).
78. F. D. Carmona, J. Ou, R. Jiménez, J. M. Collinson, Development of the cornea of true moles (Talpidae): Morphogenesis and expression of PAX6 and cytokeratins. *J. Anat.* **217**, 488–500 (2010).
79. A. Romero Jr., Cave Biology: Life in Darkness (Cambridge University Press, 2009).
80. M. Protas, W. R. Jeffery, Evolution and development in cave animals: From fish to crustaceans. Wiley Interdiscip. *Rev. Dev. Biol.* **1**, 823–845 (2012).
81. J. L. Goldberg *et al.*, Retinal ganglion cells do not extend axons by default: Promotion by neurotrophic signaling and electrical activity. *Neuron* **33**, 689–702 (2002).
82. M. Kos, B. Bulog, A. Szél, P. Röhlich, Immunocytochemical demonstration of visual pigments in the degenerate retinal and pineal photoreceptors of the blind cave salamander (Proteus anguinus). *Cell Tissue Res.* **303**, 15–25 (2001).
83. R. L. Chow, C. R. Altmann, R. A. Lang, A. Hemmati-Brivanlou, Pax6 induces ectopic eyes in a vertebrate. *Development* **126**, 4213–4222 (1999).
84. J. P. Kumar, K. Moses, Expression of evolutionarily conserved eye specification genes during Drosophila embryogenesis. *Dev. Genes Evol.* **211**, 406–414 (2001).
85. J. Zhu, S. Palliyil, C. Ran, J. P. Kumar, Drosophila Pax6 promotes development of the entire eye-antennal disc, thereby ensuring proper adult head formation. *Proc. Natl. Acad. Sci. U.S.A.* **114**, 5846–5853 (2017).
86. B. Antosova *et al.*, The gene regulatory network of lens induction is wired through Meis-dependent shadow enhancers of Pax6. *PLoS Genet.* **12**, e1006441 (2016).
87. M. E. Zuber, G. Gestri, A. S. Viczian, G. Barsacchi, W. A. Harris, Specification of the vertebrate eye by a network of eye field transcription factors. *Development* **130**, 5155–5167 (2003).
88. J. Sun *et al.*, Identification of in vivo DNA-binding mechanisms of Pax6 and reconstruction of Pax6-dependent gene regulatory networks during forebrain and lens development. *Nucleic Acids Res.* **43**, 6827–6846 (2015).
89. L. Johnson Chacko *et al.*, Neurosensory differentiation and innervation patterning in the human fetal vestibular end organs between the gestational weeks 8–12. *Front. Neuroanat.* **10**, 111 (2016).
90. J. C. Grindley, D. R. Davidson, R. E. Hill, The role of Pax-6 in eye and nasal development. *Development.* **121**, 1433–1442 (1995).
91. I. Parisi, J. M. Collinson, Regulation of Merkel cell development by Pax6. *Int. J. Dev. Biol.* **56**, 341–350 (2012).
92. N. Polisetti, G. Schlunck, T. Reinhard, PAX6 expression patterns in the adult human limbal stem cell niche. *Cells* **12**, 400 (2023).
93. K. Del Rio-Tsonis, C. H. Washabaugh, P. A. Tsonis, Expression of pax-6 during urodele eye development and lens regeneration. *Proc. Natl. Acad. Sci. U.S.A.* **92**, 5092–5096 (1995).
94. M. Madhavan *et al.*, The role of Pax-6 in lens regeneration. *Proc. Natl. Acad. Sci. U.S.A.* **103**, 14848–14853 (2006).
95. A. V. Gore *et al.*, An epigenetic mechanism for cavefish eye degeneration. *Nat. Ecol. Evol.* **2**, 1155–1160 (2018).
96. M. Stemmer, L.-N. Schuhmacher, N. S. Foulkes, C. Bertolucci, J. Wittbrodt, Cavefish eye loss in response to an early block of retinal differentiation progression. *Development* **142**, 743–752 (2015).
97. K. Katoh, D. M. Standley, MAFFT Multiple sequence alignment software version 7: Improvements in performance and usability. *Mol. Biol. Evol.* **30**, 772–778 (2013).
98. B. Q. Minh *et al.*, IQ-TREE 2: New models and efficient methods for phylogenetic inference in the genomic era. *Mol. Biol. Evol.* **37**, 1530–1534 (2020).
99. O. Chernomor, A. Von Haeseler, B. Q. Minh, Terrace aware data structure for phylogenomic inference from supermatrices. *Syst. Biol.* **65**, 997–1008 (2016).
100. D. T. Hoang, O. Chernomor, A. von Haeseler, B. Q. Minh, L. S. Vinh, UFBoot2: Improving the ultrafast bootstrap approximation. *Mol. Biol. Evol.* **35**, 518–522 (2018).
101. B. Q. Minh, M. A. T. Nguyen, A. von Haeseler, Ultrafast approximation for phylogenetic bootstrap. *Mol. Biol. Evol.* **30**, 1188–1195 (2013).
102. E. Paradis, Analysis of Phylogenetics and Evolution with R (Springer, New York, ed. 2, 2012).
103. L. J. Revell, Phytools 2.0: An updated R ecosystem for phylogenetic comparative methods (and other things). *PeerJ* **12**, e16505 (2024).
104. R. Desper, O. Gascuel, Fast and accurate phylogeny reconstruction algorithms based on the minimum-evolution principle. *J. Comp. Biol.* **9**, 687–705 (2002).
105. W. E. Duellman, L. Trueb, Biology of Amphibians (JHU Press, 1994).
106. C. C. Nice *et al.*, Extensive admixture among karst-obligate salamanders reveals evidence of recent divergence and gene exchange through aquifers. *Ecol. Evol.* **15**, e70785 (2025).
107. R. M. Green, C. L. Leach, N. Hoehn, R. S. Marcucio, B. Hallgrímsson, Quantifying three-dimensional morphology and RNA from individual embryos. *Dev. Dyn.* **246**, 431–436 (2017).
108. A. Veith, A. B. Baker, A rapid, nondestructive method for vascular network visualization. *BioTechniques* **69**, 443–449 (2020).
109. R Core Team, R: A Language and Environment for Statistical Computing (R Foundation for Statistical Computing, Vienna, Austria, 2023), https://www.R-project.org/.